30th European Conference on Acoustic Emission Testing & 7th International Conference on Acoustic Emission
University of Granada, 12-15 September 2012
www.ndt.net/EWGAE-ICAE2012/

Influence of Internal Discontinuities on Ultrasonic Signal Propagation in Carbon Fiber Reinforced Plastics

Markus G. R. SAUSE [1], Siegfried HORN [1]

[1] Institute for Physics, University of Augsburg; Augsburg, Germany
Phone: +49 821 5983238, Fax: +49 821 5983411; e-mail: markus.sause@physik.uni-augsburg.de; horn@physik.uni-augsburg.de

Abstract
Numerical and experimental studies were performed to investigate acoustic emission signal propagation in Aluminum and CFRP plates. For the case of thin plates, Lamb waves are the dominating mode of propagation for ultrasonic waves. The interpretation of Lamb waves is one of the main challenges for valid source localization or identification procedures. Naturally, the lateral size and the thickness of the plate have a significant impact on the propagation behavior of guided waves. While these geometric dimensions can be understood as boundary conditions, distortions of wave patterns caused by internal discontinuities are more difficult to understand. Inter-ply delamination is often encountered in carbon fiber reinforced plastics as consequence of impact damage or manufacturing error. Other types of inhomogeneities are embedded metallic parts like rivets or bolts. The current study presents results of finite element calculations to investigate the influence of those discontinuities on the propagation behavior of distinct Lamb wave modes. Simulation results are compared to measurements of the out-of-plane displacement using Laservibrometry in order to validate the numerical approach. While inter-ply delamination has minor influence on the Lamb wave propagation, the interaction with holes and rivets results in significant distortions of the wave pattern.

Keywords: carbon fiber composite, finite element method, acoustic emission, Lamb waves

1. Introduction

Among the class of engineering materials carbon fiber reinforced plastics (CFRP) show extraordinary high strength to weight and stiffness to weight ratio. This makes them ideal materials for construction of aircrafts, high-performance cars or sporting goods. The design of CFRP structures relies on the anisotropy of the elastic properties caused by the alignment of carbon fibers. While this anisotropy is advantageous for constructional aspects, it causes major challenges for non-destructive evaluation of these structures. Such monitoring of the structural integrity of CFRP is often done by acoustic emission (AE) analysis or active guided wave monitoring. Both methods rely on the propagation of acoustic waves in flat, plate-like structures. Plate waves are the dominant mode of wave propagation in those structures, which are also known as Lamb waves [1]. The infinite number of Lamb wave modes, which can exist within a plate is of two types. One type shows symmetric and one type shows anti-symmetric motion with respect to the mid-plane of the plate. However, the types of modes found most often in thin-walled CFRP structures are the fundamental symmetric mode (S_0) and anti-symmetric mode (A_0), often referred to as extensional and flexural mode. Lamb wave propagation in undamaged CFRP has been investigated extensively before [2-5]. Scattering of Lamb waves at internal damage, like micro-cracks or delamination, is the key principle for structural health monitoring (SHM) of CFRP by guided wave testing [6]. The impact of such discontinuities on acoustic emission analysis has been investigated less. Since Lamb wave propagation is the carrier of information on AE source activity in the material, distortion of information due to interaction of Lamb waves with internal discontinuities is closely related to the question of reliability of the information. Changes of modal intensity or occurrence of alternative propagation paths due to metallic enclosures can readily affect source localization accuracy or complicate source identification procedures. The purpose of the current study is the investigation of changes in the detected Lamb waves due to internal discontinuities by a numerical method. Using finite element modeling (FEM), the interaction of Lamb waves with

discontinuities is easily visualized and it was recently demonstrated that this approach yields results consistent with experiments [5, 7].

2. Model configuration

The finite element method used within this study is comprehensively described in earlier publications [5, 8, 9]. Thus the reader is referred to these publications for any details that are beyond the description unique to the current approach. All calculations were performed within the software package COMSOL and all descriptions below follow the way of implementation within the module Structural Mechanics in this software package.
The model setup used in this study is shown in figure 1. A rectangular plate of 200 mm × 200 mm size and 1 mm thickness is used as propagation medium. Elastic properties of unidirectional CFRP plate are used as given in table 1. Fiber direction of the unidirectional lamina is oriented along the 0° axis as noted in figure 1. Two symmetry planes were chosen to reduce the volume modeled to one quarter of the overall volume. The symmetry planes are the yz- and xz-plane with respect to the origin of the coordinate system.

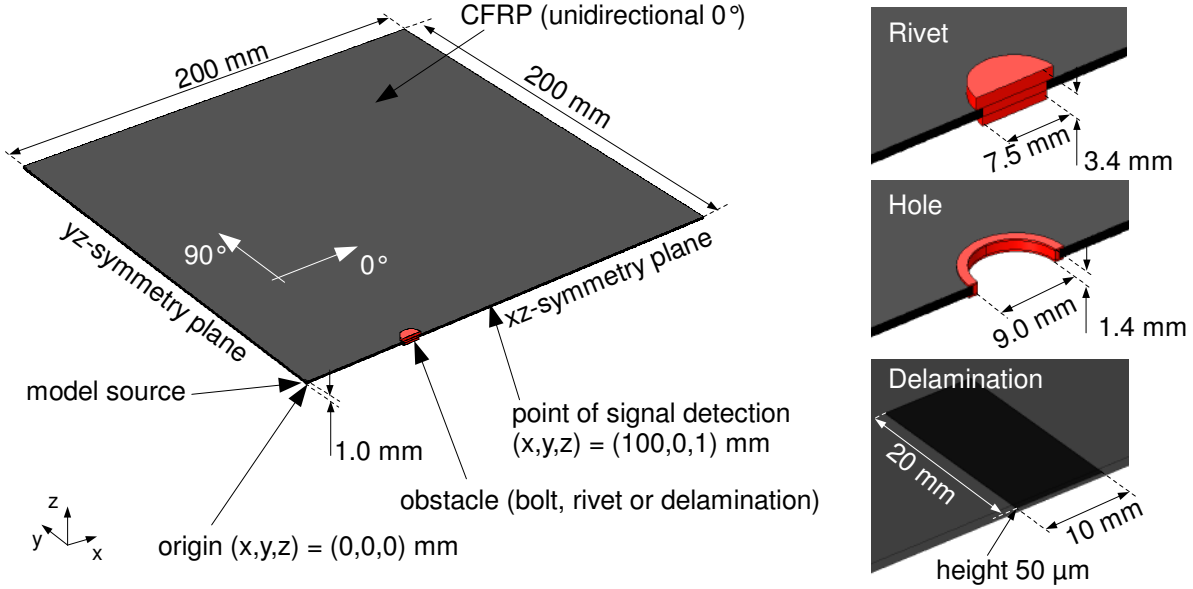

Figure 1. 3-dimensional model setup used for simulation of Lamb wave propagation including details for bolt, rivet and delamination dimensions.

As acoustic emission source a point couple was chosen following [10]. As demonstrated in [11] such point couples can be used to excite particular fundamental Lamb wave modes in isotropic plates. In contrast to complex source models based on micromechanical considerations [5, 8], point couples are computationally more efficient to investigate Lamb wave propagation in larger structures. The position of the point couple was chosen at (x, y, z) = (0.00, 0.00, 0.53) mm, slightly asymmetric with respect to the mid-plane of the plate, to excite a reasonable amount of S_0 and A_0 Lamb wave modes at the same time. The length of the dipole (oriented in x-direction) was chosen to be 200 µm. A linear ramp function with excitation time $t_e = 1\,\mu s$ and maximum force $F_{\max} = 3\,N$ is used.

$$F(t) = \begin{cases} F_{\max} \cdot (t/t_e) & t \le t_e \\ F_{\max} & t > t_e \end{cases} \quad (1)$$

The obstacle was placed with midpoint at a distance of 50 mm in x-direction to the source. Details of the dimensions chosen for a rivet, a bordered hole and inter-ply delamination are found in figure 1. Each of these obstacles refers to one prototype of discontinuity. Rivets and bolts are through-thickness metallic enclosures that allow direct transmission of elastic waves, but are expected to cause wave scattering due to their acoustic impedance mismatch. A hole is also a through-thickness obstacle, but does not allow transmission of elastic waves. In contrast, inter-ply delamination is an in-plane discontinuity that weakens the local bending stiffness of the plate. All metallic parts (marked in red in figure 1) are modeled as high-strength alloy steel parts, with elastic properties as listed in table 1. All signals are evaluated at 100 mm distance to the AE source in 0°, 45° and 90° propagation direction as z-displacement of the plate.

Table 1. List of elastic properties used for finite element modeling.

	Density [kg/m³]	Poisson-Ratio	Elasticity Constants [GPa]
T800/913 (unidirectional)	1550	-	C_{11}=154.0 C_{12}= C_{13}=3.7 C_{22}= C_{33}=9.5 C_{23}=5.2 C_{44}=2.5 C_{66}= C_{55}=4.2
High strength alloy steel	7850	0.33	200.0
AlMg3	2660	0.33	70.0

For accurate resolution of calculated signals, a maximum element size of 1.0 mm edge length was chosen for tetrahedral mesh elements with quadratic order of the geometry shape functions. To resolve geometric details in narrow regions the mesh was refined down to a minimum edge length of 5 µm in such areas. The temporal resolution was chosen to be 100 ns and results were calculated for the first 100 µs after signal excitation. Convergence of simulation results with respect to mesh resolution and temporal resolution was previously checked by subsequent refinement. To this end mesh resolution was increased to 0.5 mm edge length and temporal resolution was increased to 5 ns. Results of these calculations were found to have a coherence level ≥ 0.998 to the current settings within the frequency range between 1 kHz and 2 MHz.

3. Experimental

In order to validate the finite element modeling approach we compare simulation results to measured signals of pencil lead breaks. For those experiments a 2 m × 1 m wide and 3 mm thick AlMg3 aluminium plate was used. Measurements were conducted using a Laservibrometer (model OFV-5000) with a displacement decoder unit (model DD-900). Pencil lead breaks were applied at a distance of 100 mm to the point of detection. The signals were recorded using a data acquisition card (model PCI-2) with 40 dB preamplification and bandpass range between 20 kHz and 1 MHz. For numerical modeling, we used a plate size of 0.50 m × 0.75 m with 3 mm thickness and symmetry boundary conditions at the yz- and xz-plane. The lateral size of the plate is large enough to avoid interference of the calculated signal with edge reflections within the first 125 µs. The elastic properties used are given in table 1. Mesh resolution and temporal resolution correspond to the settings given in section 2. To simulate pencil lead breaks, a monopole point source was defined at the plate surface acting in out-of-plane direction. As source function, equation (1) was used, which was found to be a suitable analytical description for modeling of pencil lead breaks [12].

The measured out-of-plane displacement signal and the out-of-plane velocity signal are compared to calculated signals in figure 2-a and figure 2-b, respectively. The calculated signal was filtered by a 4th order Butterworth high-pass filter to take into account the experimentally used high-pass setting. Within the range of scatter of the experimental signals the simulation results show good agreement to the Laservibrometer signals in shape and amplitude. Thus, the proposed finite element approach is expected to show sufficient predictive capability for the intended analysis of Lamb wave propagation.

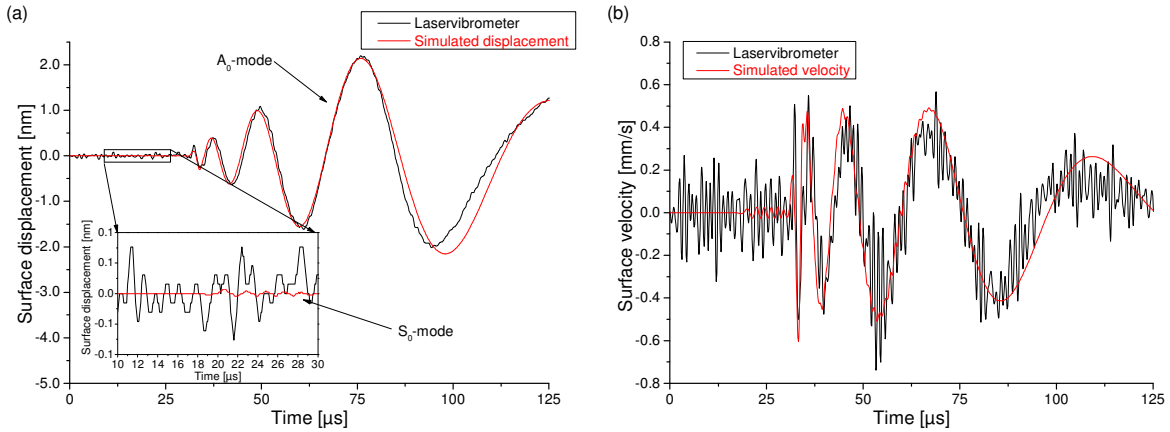

Figure 2. Comparison of simulation results and measurement of out-of-plane displacement (a) and out-of-plane velocity (b) using Laservibrometer for signal of pencil lead breakage at distance of 100 mm.

4. Influence of discontinuities

In the following the influence of the modeled discontinuities is investigated. Figure 3 shows the Choi-Williams distribution (CWD) of the calculation result for signal propagation along the 0° axis of the unidirectional CFRP plate [13]. The CWD in figure 3-a uses a different color, frequency and time range than figure 3-b, which is used to visualize the S_0-mode at the initial part of the signal. To identify particular Lamb wave modes, the dispersion curves of the fundamental modes were calculated by the software package provided by [14]. As indicated by the superimposed dispersion curves for the S_0-mode at 100 mm and 300 mm source distance, the S_0-mode is reflected at the edge of the plate in x-direction and is detected twice. The shape of the A_0-mode shown in figure 3-b agrees well with the calculated result of the dispersion curve for 100 mm distance. The calculation result for pure CFRP in figure 3 will act as a reference case to evaluate the influence of discontinuities. A comparison of the calculated wave-field will be made in section 5.

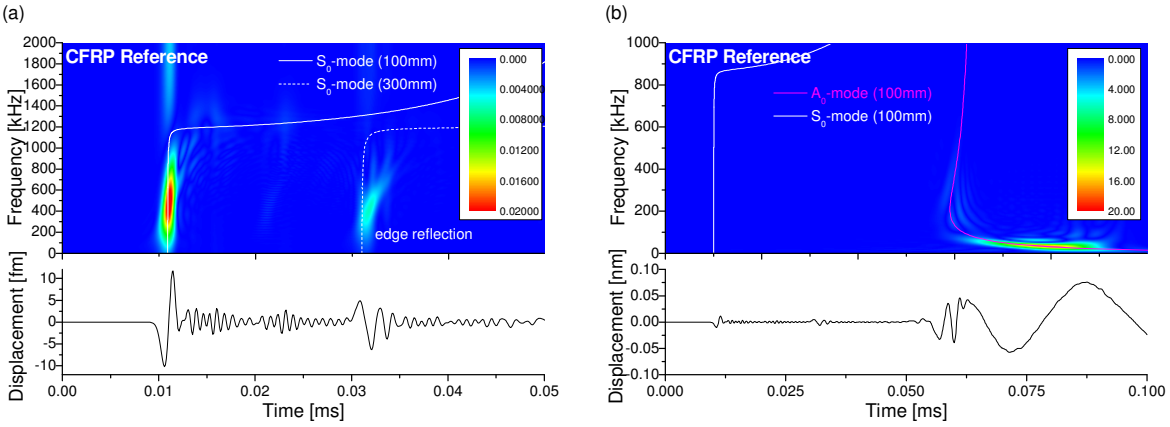

Figure 3. Simulation results of signal propagation at 100 mm distance along 0° direction in unidirectional CFRP. Truncated time scale shows S_0-mode (a) and full time scale shows A_0-mode (b).

4.1 Bolts and rivets

Bolts and rivets are commonly used as fasteners in CFRP structures and are frequently encountered during testing of realistic structures. The calculation result for signal propagation in the presence of such obstacles is shown in figure 4 with time, frequency and coefficient range settings slightly different to figure 3. As observed from figure 4-a, shape and intensity of the S_0-mode are influenced by the presence of the rivet within the propagation path. The intensity is less than for the reference structure. On one hand this is caused by the acoustic transmission coefficient (0.75) of the CFRP-metal and metal-CFRP interface in 0° direction calculated under the assumption of planar wave incidence. On the other hand, interfaces are likely to cause modal conversion. For the current case, a significant part of the incident S_0-mode is converted to an A_0-mode radiating away from the rivet (cf. also fig. 7 and fig. 8). This causes an additional emission of an A_0-mode that is ahead of the A_0-mode originally emitted by the point source. Thus, determination of the correct arrival time of the A_0-mode with respect to the point source is almost impossible.

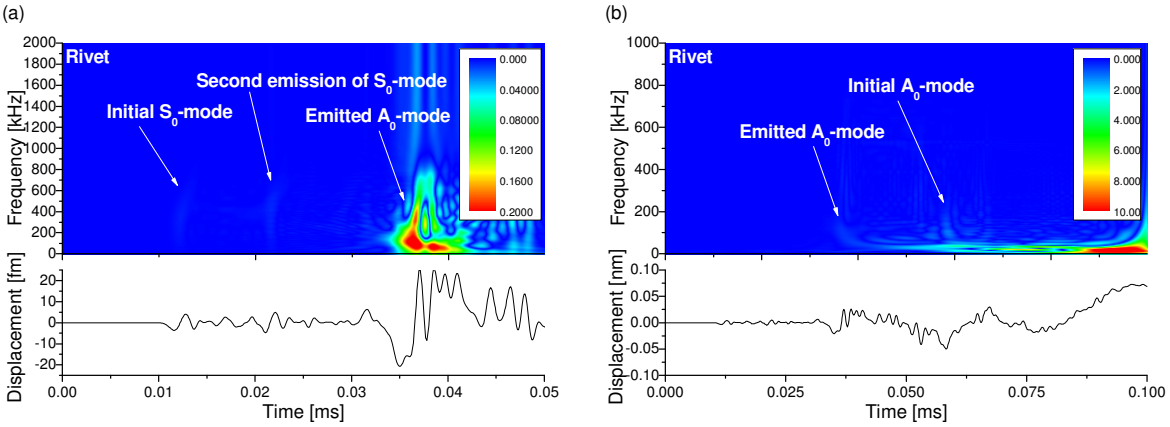

Figure 4. Simulation results of signal propagation at 100 mm distance along 0° direction in unidirectional CFRP with included rivet. Truncated time scale shows S_0-mode (a) and full time scale shows A_0-mode (b).

4.2 Inter-ply Delamination

Inter-ply delamination is one of the most common types of CFRP damage since it is often caused by impact damage or as manufacturing error. During mechanical testing of CFRP structures, delamination can evolve step by step and can affect the elastic properties along the signal propagation path. Thus, the influence of delamination on the detected AE signals is of large interest. Figure 5 shows the calculated CWDs with settings identical to figure 3. For the S_0-mode there are only negligible differences observed to the reference case as shown in figure 5-a. Since propagation of the S_0-mode is dominated by the in-plane stiffness, this can readily be explained. Thinking of a multi-layer specimen composed of 950 µm CFRP and 50 µm air the in-plane stiffness is as close as 95 % of the stiffness of a 1000 µm CFRP plate. Larger influence is observed for the propagation behavior of the A_0-mode as seen from figure 5-b. Shape and intensity of the A_0-mode differ from the signal of figure 3-b, which is caused by the change of local bending stiffness introduced by the delamination length of 10 mm.

4.3 Holes

Holes in CFRP are another type of acoustic obstacle often encountered in technical CFRP structures. These can originate from drilling processes or represent serious damage after high-velocity impacts. As shown in the CWDs in figure 6 with settings identical to figure 3, the influence of this kind of obstacle is more severe than the influence of delamination. As seen in figure 6-a, presence of the through-thickness hole causes less intense transmission of the

initial S_0-mode. Also, the shape of the hole causes a second emission of a S_0-mode with a virtual source position located at the center of the hole. This process is observed in more detail in figures 7 and 8 in section 5. For the propagation of the A_0-mode a similar influence like for delamination was found. This is explained by the fact, that both obstacles have a similar dimension in x-direction. As soon as the wavelength of the A_0-mode becomes sufficiently larger than the structure, there is no interaction. Thus, only the short wavelengths of the A_0-mode (initial part) are affected by the presence of the hole and are scattered at the obstacle.

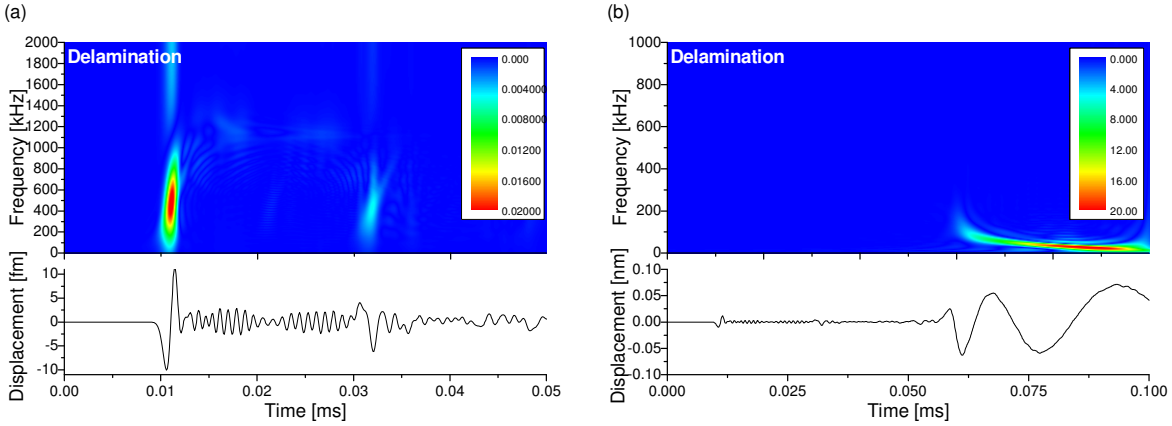

Figure 5. Simulation results of signal propagation at 100 mm distance along 0° direction in unidirectional CFRP with embedded inter-ply delamination. Truncated time scale shows S_0-mode (a) and full time scale shows A_0-mode (b).

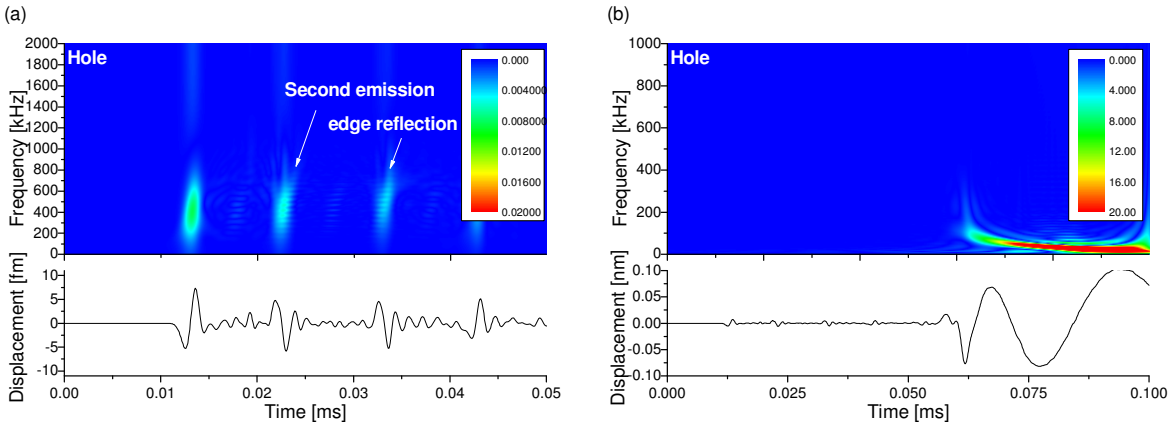

Figure 6. Simulation results of signal propagation at 100 mm distance along 0° direction in unidirectional CFRP with hole. Truncated time scale shows S_0-mode (a) and full time scale shows A_0-mode (b).

5. Discussion of results

In the present study the interaction of Lamb wave modes with different types of internal discontinuities in unidirectional CFRP plates were investigated by means of finite element modeling. For evaluation of the signals an unidirectional CFRP plate was chosen as propagation medium, since this has a maximal elastic anisotropy. The wave fields obtained for the reference case (without obstacles), an included rivet, inter-ply delamination and hole are shown in figures 7 and 8 for two distinct times $t = 20\,\mu s$ and $t = 40\,\mu s$ after signal excitation. As mentioned in the previous section, rivets and holes show a stronger interaction with the incident Lamb waves than a delamination. The interaction of obstacles with the S_0-mode is visualized best in the wave-fields in figure 7. Both, rivet and hole cause a strong secondary A_0-mode with almost circular radiation pattern around the center-point of the

obstacle. The only explanation for this is a modal conversion of the primary S_0-mode to a secondary A_0-mode, since the primary A_0-mode did not arrive at the obstacle for $t < 20\ \mu s$. For the hole, the incident primary S_0-mode is also partially deflected at the inner boundary of the hole, which causes a strong secondary S_0-mode (see figure 7-d). For the delamination case only weak interaction with the S_0-mode is found.

In figure 8, the wave field for $t = 40\ \mu s$ shows the interaction of the A_0-mode with the obstacles. Similar as for the incident S_0-mode, the A_0-mode is partially reflected at the rivet and at the hole. Both obstacles cause similar reflection of the A_0-mode, since both are through thickness discontinuities affecting the bending stiffness of the plate. Again only weak interaction is found for the modeled delamination and the A_0-mode as shown in figure 8-c.

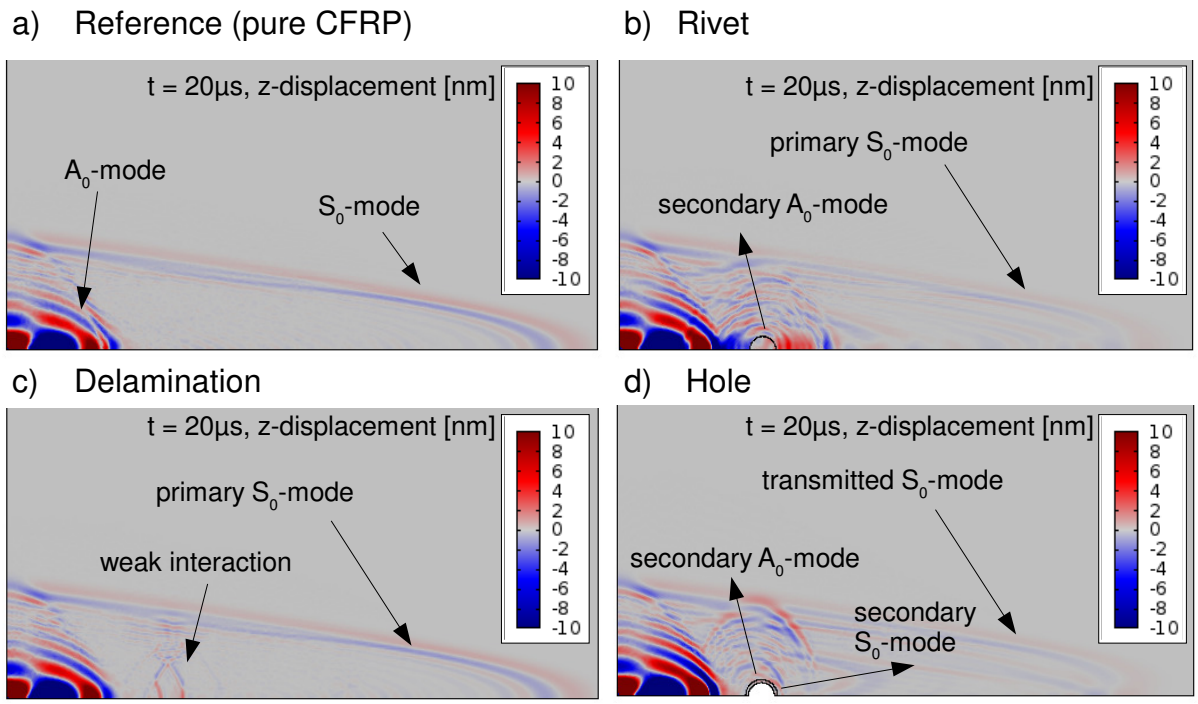

Figure 7. Comparison of simulated wave fields z-displacement for reference (a), rivet (b), delamination (c) and hole (d) at $t = 20\ \mu s$ after signal excitation.

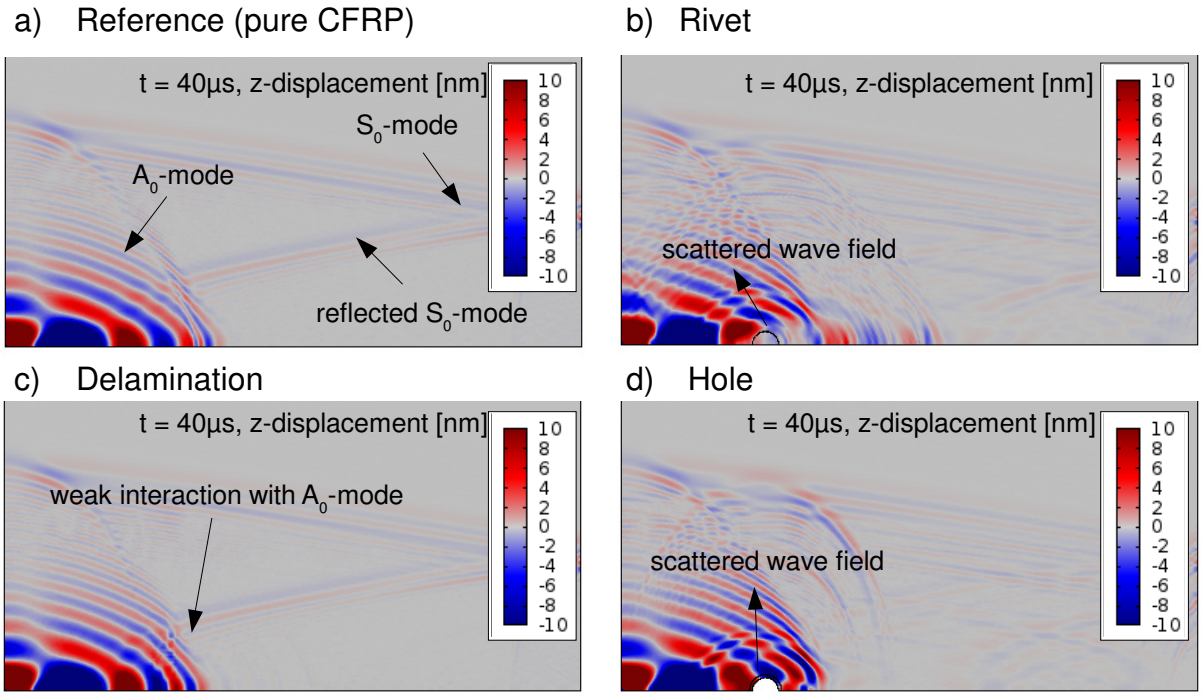

Figure 8. Comparison of simulated wave fields z-displacement for reference (a), rivet (b), delamination (c) and hole (d) at t = 40 µs after signal excitation.

In order to investigate the influence on AE analysis, the calculated signals are processed in a similar way as experimental signals. Thus, typical AE features are extracted from the signals and arrival times of S_0-mode and A_0-mode are calculated for a distance of 100 mm in all propagation directions. Table 3 lists all AE parameters and arrival times of the four cases studied. For calculation of signal energies and signal amplitude an artificial sensor sensitivity of $4.5 \cdot 10^9$ V/m was assumed.

The definition of features is based on the basic properties derived from the signal in time domain $U(t)$ and in frequency domain $\widetilde{U}(f)$ as shown in figure 9-a and 9-b, respectively. U_{max} is the maximum signal amplitude, as seen in figure 9-a, while the absolute energy is derived from the integral of $U(t)^2$ within the investigated time of 100 µs. f_{peak} defines the frequency position of maximum FFT-magnitude as seen in figure 9-b, while $f_{centroid}$ is defined in table 2. Definition of the different Partial Power features is given in table 2 as well.

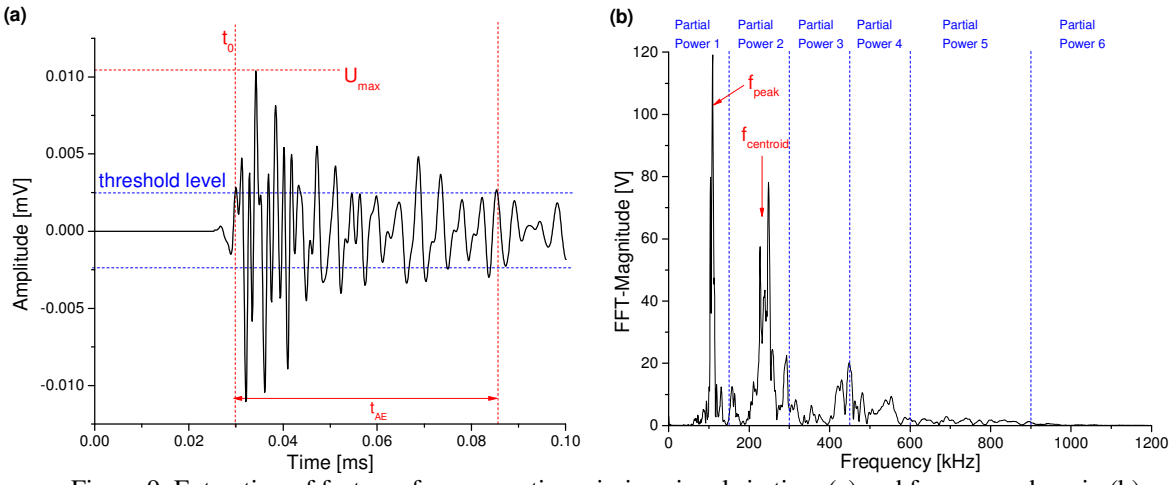

Figure 9. Extraction of features from acoustic emission signals in time (a) and frequency domain (b).

Table 2. Definition of AE features.

AE feature	Definition
Amplitude [mV]	U_{max}
Amplitude [dB]	U_{max} with ref. to 1µV
Absolute energy [fJ]	$E = \int_0^{t_{AE}} U(t)^2/10k\Omega\, dt$
Peak frequency [kHz]	f_{peak}
Frequency centroid [kHz]	$f_{centroid} = \frac{\int f \cdot \tilde{U}(f) df}{\int \tilde{U}(f) df}$
Partial Power 1 [%]	$\frac{\int_{f_1}^{f_2} \tilde{U}^2(f) df}{\int_{0kHz}^{1200kHz} \tilde{U}^2(f) df}$ PP1: f1 = 0 kHz; f2 = 150 kHz PP2: f1 = 150 kHz; f2 = 300 kHz PP3: f1 = 300 kHz; f2 = 450 kHz PP4: f1 = 450 kHz; f2 = 600 kHz PP5: f1 = 600 kHz; f2 = 900 kHz PP6: f1 = 900 kHz; f2 = 1200 kHz
Partial Power 2 [%]	
Partial Power 3 [%]	
Partial Power 4 [%]	
Partial Power 5 [%]	
Partial Power 6 [%]	

Table 3. Values of AE features extracted from the calculated signals in various propagation directions.

	Reference			Rivet			Delamination			Hole		
AE feature	0°	45°	90°	0°	45°	90°	0°	45°	90°	0°	45°	90°
Amplitude [mV]	342.4	30.5	24.7	327.8	71.7	39.4	322.0	35.1	24.4	463.8	57.1	47.9
Amplitude [dB]	111	90	88	110	97	92	110	91	88	113	95	94
Absolute energy [fJ]	11689	862	180	11936	3867	1314	17693	1298	292	35316	3612	1469
Peak frequency [kHz]	39	127	293	39	88	293	39	98	293	29	146	253
Frequency centroid [kHz]	396	425	869	673	436	482	427	636	537	659	571	498
Partial Power 1 [%]	59.5	38.6	15.9	59.1	35.8	14.1	75.9	35.7	15.9	75.6	32.8	18.1
Partial Power 2 [%]	13.3	21.1	18.4	12.4	21.3	23.8	11.1	20.1	18.5	8.6	28.1	19.3
Partial Power 3 [%]	13.7	17.7	17.9	7.3	21.0	32.0	4.0	12.7	20.2	6.0	14.3	23.3
Partial Power 4 [%]	7.0	9.2	8.9	7.7	11.3	12.3	2.7	9.1	15.3	3.0	10.9	17.3
Partial Power 5 [%]	4.9	1.1	23.3	9.9	9.5	16.4	3.6	19.9	28.5	4.0	11.6	19.1
Partial Power 6 [%]	1.6	2.3	15.5	3.6	1.2	1.3	2.6	2.4	1.6	2.7	2.1	2.8
Arrival time A_0-mode [µs]	60.8	60.8	85.0	36.9	54.6	61.0	60.8	61.2	85.8	61.7	61.4	85.5
Arrival time S_0-mode [µs]	11.1	44.0	51.1	12.6	44.3	50.6	11.1	43.4	50.8	13.3	45.0	50.3

Arrival times of S_0-mode and A_0-mode are picked from the CWDs following the method introduced by Hamstad et al. [15]. Thus, arrival of the mode is picked as the time of maximum coefficient intensity of the respective mode at a constant frequency (500 kHz in the current case).

5.1 Influence on source localization accuracy

Based on the maximum deviation of 2.3 µs to the reference case of the calculated arrival time of the S_0-mode, a corresponding error of localization in the range of several centimeters can be expected. The estimation is based on the calculated group velocity of 10000 m/s of the S_0-mode in 0° propagation direction. However, for an observation angle different than 0°, the influence was found to be less than 1 µs reflecting the fact that the signal does not propagate through the obstacle. A drastically larger influence was found for the arrival time of the A_0-mode. Due to modal conversion at the rivet, the arrival of the first detectable A_0-mode is 23.9 µs ahead to the reference case. However, this is not the arrival of the primary A_0-mode as discussed before. For the remaining cases studied (hole and delamination), the arrival times of the A_0-mode are within 0.9 µs difference to the reference case. Consequently, for localization

methods using arrival times of both fundamental Lamb wave modes, the observed difference in arrival time of the A_0-mode might have a large impact as well.

5.2 Influence on source identification methods

For source identification procedures one approach is the use of parameter based pattern recognition [9, 5, 7]. Since cracks and delamination are likely to evolve between AE source positions and the position of detection during specimen loading, their influence on the transmitted Lamb waves has to be understood thoroughly.
From the list of calculated features given in table 2, some were found to deviate more than 70 % from the reference case. While this may seem unacceptable high, it is worth noting that the deviation of the majority of the features (> 75 %) to the reference case is ≤ 10 %. For pattern recognition methods, this is a typical experimentally encountered distribution range for an individual feature. In comparison to the distinct feature values of one particular source type in CFRP (see e.g. [9, 5, 7]), the feature range observed here is quite acceptable. Thus the applicability of these approaches is not seriously affected by the presence of delamination or other obstacles within the propagation path.

6. Conclusion

Within this study the influence of internal discontinuities on signal propagation of Lamb waves was investigated. To this end a FEM approach was used, which was found to yield appropriate results for prediction of magnitude and shape of Lamb waves based on a comparison to measurements using Laservibrometry.
For the present study a unidirectional reinforced plate was studied, with internal discontinuities (bolt, hole, delamination) located at 0° orientation of the fibers. This configuration was chosen, since complementary studies with obstacles placed in 90° orientation to the fibers confirmed that the influence of the obstacles is largest in the 0° case.
Overall, a significant influence of all discontinuities was observed, that is well detectable with piezoelectric sensors, and thus a feasible approach for SHM utilizing guided wave monitoring. For AE analysis, the largest impact is expected for source localization routines, since obstacles like bolts or holes can act as virtual AE source caused by modal conversion effects. This drastically alters the emitted wave field of the original source and may even affect the initial arrival time of distinct wave modes, causing substantial errors during source localization. Also, energetic features and frequency features extracted from the Lamb wave signals are influenced by the presence of internal discontinuities. In some cases, the influence on a particular feature value was found to be drastic. But in total, the overall range of values of the extracted features is well comparable to ranges where pattern recognition approaches still can lead to valid classifications of source mechanisms.

References

1. H Lamb, 'On Waves in an Elastic Plate', Proceedings of the Royal Society of London Series A Containing Papers of a Mathematical and Physical Character, Vol 93, pp 114-128, 1917.
2. M Lowe, ‘Matrix techniques for modeling ultrasonic waves in multilayered media’, IEEE Transactions on Ultrasonics Ferroelectrics and Frequency Control, Vol 42, No 4, pp 525-542, 1995.
3. M Castaings, C Bacon, B Hosten, M Predoi, ‘Finite element predictions for the dynamic response of thermo-viscoelastic material structures’, Journal of the Acoustical Society of America, Vol 115, No 3, pp 1125-1133, 2004.

4. L Wang, F Yuan, ‘Group velocity and characteristic wave curves of Lamb waves in composites: Modeling and experiments’, Composites Science and Technology, Vol 67, pp 1370-1384, 2007.
5. M Sause, S Horn, ‘Simulation of acoustic emission in planar carbon fiber reinforced plastic specimens’, Journal of Nondestructive Evaluation, Vol 29, No 2, pp 123-142, 2010.
6. A Raghavan, C Cesnik, ‘Review of Guided-wave Structural Health Monitoring’, The Shock and Vibration Digest, Vol 39, pp 91-114, 2007.
7. M Sause, T Müller, A Horoschenkoff, S Horn, ‘Quantification of failure mechanisms in mode-I loading of fiber reinforced plastics utilizing acoustic emission analysis’, Composite Science and Technology, Vol 72, pp 167-174, 2012.
8. M Sause, S Horn, ‘Simulation of Lamb Wave Excitation for Different Elastic Properties and Acoustic Emission Source Geometries’, Journal of Acoustic Emission, Vol 28, pp 109-121, 2010.
9. M Sause, ‘Identification of failure mechanisms in hybrid materials utilizing pattern recognition techniques applied to acoustic emission signals’, PhD-Thesis, mbv-Verlag, Berlin, 2010.
10. J Gary, M Hamstad, ‘On the Far-field Structure of Waves Generated by a Pencil Lead Break on a Thin Plate’, Journal of Acoustic Emission, Vol 12, No 3-4, pp 157-170, 1994.
11. M Hamstad, A O’Gallagher, J Gary, ‘A Wavelet Transform Applied To Acoustic Emission Signals: Part 1: Source Identification’, Journal of Acoustic Emission, Vol 20, pp 39-61, 2002.
12. M Sause, ‘Investigation of Pencil-Lead Breaks as Acoustic Emission Sources’, Journal of Acoustic Emission, Vol 29, pp 184-196, 2011.
13. H Choi, W Williams, ‘Improved Time-Frequency Representation of Multicomponent Signals Using Exponential Kernels’, IEEE Transactions on Acoustics, Speech and Signal Processing, Vol 37, No 6, pp 862-872, 1989.
14. R Zeyde, ‘Notes on orthotropic Lamb waves’, Technion - Israel Institute of Technology, http://mercurial.intuxication.org/hg/elasticsim/, 2010.
15. M Hamstad, ‘Comparison of Wavelet Transform and Choi-Williams Distribution to Determine Group Velocities for Different Acoustic Emission Sensors’, Journal of Acoustic Emission, Vol 26, pp 40-59, 2008.